Journal of Engineering Mathematics **36:** 277–287, 1999.

Steady flow past an oblate spheroid at small Reynolds numbers

R. S. ALASSAR and H. M. BADR
[1]*Department of Mathematical Sciences, King Fahd University of Petroleum and Minerals, Dhahran 31261, Saudi Arabia*
[2]*Mechanical Engineering Department, King Fahd University of Petroleum and Minerals, Dhahran 31261, Saudi Arabia*

Received 26 February 1998; accepted in revised form 5 February 1999

Abstract. The problem of uniform steady viscous flow over an oblate spheroid is solved in the low-Reynolds-number range $0{\cdot}1 \leqslant \mathrm{Re} \leqslant 1{\cdot}0$. The full Navier-Stokes equations are written in the stream function-vorticity form and solved numerically by means of the series-truncation method. Spheroids having axis ratio ranging from 0·245 to 0·905 are considered. The obtained drag coefficients are compared with previous analytical formulae which were based on the solution of the linearized Stokes equations. As expected, the deviation between the present results and the analytical formulae is small for low-Re flows, however, it increases with the increase of Re. The present results provide a measure for establishing the range of validity of the analytical solutions.

Key words: uniform steady flow, Legendre functions, oblate spheroids, series-truncation method.

1. Introduction

A considerable amount of research has been published on axisymmetric flows past spheres. In many situations, however, the shape of the particles contained in an infinite fluid is not perfectly spherical. Aerosols, for example, are oblate spheroidal in shape. According to Lawrence and Weinbaum [1], a new behavior of the drag was discovered. While investigating the oscillatory motion over oblate spheroids, they found that the force was not a simple quadratic function in half-integer powers of the frequency as in the classical solution of Stokes for a sphere, and the force for an arbitrary velocity contained a new memory integral whose kernel differed from the classical behavior derived by Basset for a sphere. Payne and Pell [2] neglected the inertia terms and obtained formulae for the drag on bodies of various shapes including oblate spheroids. Breach [3] modified these formulae by using the two classical methods, those of Stokes and Oseen, for finding approximations to viscous streaming at low Reynolds numbers. The drag formulae by Payne and Pell [2] and Breach [3] are only valid for small Reynolds numbers.

In this study, a series-truncation method, where the stream function and the vorticity are expanded in terms of Legendre polynomials, is used to solve the problem of uniform steady flow over oblate spheroids for Reynolds number $\leqslant 1$. The results obtained from solving the full Navier-Stokes equations are used to check the range of validity of the available analytical solutions which are based on the solution of Stokes equations (nonlinear terms are neglected).

2. Formulation of the problem

Consider the problem of uniform steady incompressible axisymmetric flow over an oblate spheroid with major and minor axes of 2a and 2b as shown in Figure 1. To suit the geometry of

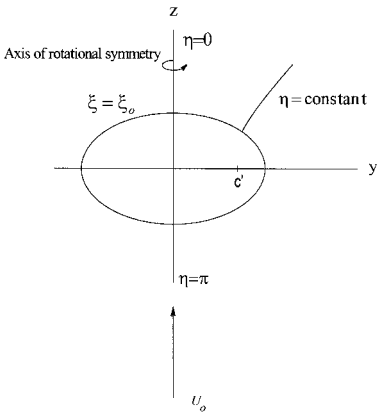

Figure 1. The Coordinate system.

the problem, we transform the Navier-Stokes equations into the oblate-spheroidal coordinates system (ξ, η, φ) using the relations

$$\begin{aligned} x &= c' \cosh\xi \sin\eta \cos\varphi, \\ y &= c' \cosh\xi \sin\eta \sin\varphi, \\ z &= c' \sinh\xi \cos\eta, \end{aligned} \tag{1}$$

where c' is the focal distance. These equations, upon introduction of the stream function ψ, and vorticity ζ, take the following dimensionless form

$$\cosh\xi \sin\eta(\sinh^2\xi + \cos^2\eta)\zeta + \cosh\xi \frac{\partial}{\partial\xi}\left(\frac{1}{\cosh\xi}\frac{\partial\psi}{\partial\xi}\right) + \sin\eta \frac{\partial}{\partial\eta}\left(\frac{1}{\sin\eta}\frac{\partial\psi}{\partial\eta}\right) = 0, \tag{2}$$

$$\begin{aligned} &\frac{\partial\psi}{\partial\eta}\frac{\partial}{\partial\xi}\left(\frac{\zeta}{\cosh\xi\sin\eta}\right) - \frac{\partial\psi}{\partial\xi}\frac{\partial}{\partial\eta}\left(\frac{\zeta}{\cosh\xi\sin\eta}\right) \\ &\quad = \frac{2}{\mathrm{Re}}\left\{\frac{\partial}{\partial\xi}\left[\frac{1}{\cosh\xi}\frac{\partial}{\partial\xi}(\cosh\xi\zeta)\right] + \frac{\partial}{\partial\eta}\left[\frac{1}{\sin\eta}\frac{\partial}{\partial\eta}(\sin\eta\zeta)\right]\right\}. \end{aligned} \tag{3}$$

The stream function is related to the dimensionless velocity components (w_ξ, w_η) by

$$\frac{\partial\psi}{\partial\eta} = \sqrt{\sinh^2\xi + \cos^2\eta}\cosh\xi\sin\eta w_\xi, \qquad \frac{\partial\psi}{\partial\xi} = -\sqrt{\sinh^2\xi + \cos^2\eta}\cosh\xi\sin\eta w_\eta, \tag{4}$$

and the vorticity is defined in the usual way as the curl of the velocity vector.

In the above equations, the dimensionless variables are related to the dimensional ones by: $\psi = \psi'/U_o c'^2$, $\zeta = (\zeta' c'/U_o)$, $w = (w'/U_o)$, with U_o being the free-stream velocity and primes denote dimensional quantities. The Reynolds number Re is defined as $\mathrm{Re} = (\rho U_o(2c')/\mu)$, where ρ is the fluid density, and μ is the coefficient of viscosity.

The boundary conditions to be satisfied are the no-slip and impermeability conditions on the surface of the spheroid and the free-stream conditions away from it. These can be expressed as

$$\psi = \frac{\partial\psi}{\partial\eta} = \frac{\partial\psi}{\partial\xi} = 0 \quad \text{at } \xi = \xi_o, \tag{5}$$

$$\frac{\partial\psi}{\partial\xi} \to \tfrac{1}{2}\sinh 2\xi \sin^2\eta \quad \text{and} \quad \frac{\partial\psi}{\partial\eta} \to \tfrac{1}{2}\cosh^2\xi \sin 2\eta \quad \text{as } \xi \to \infty. \tag{6}$$

The parameter ξ_o defines the surface of the spheroid and is related to the axis ratio (b/a) by: $\xi_o = \tanh^{-1}(b/a)$. A perfect sphere would be represented by $\xi_o \to \infty$ whereas a flat circular disk would be represented by $\xi_o = 0$. The conditions in Equation (6) lead to,

$$\psi \to \tfrac{1}{2}\cosh^2\xi \sin^2\eta \quad \text{as } \xi \to \infty. \tag{7}$$

The flow away from the oblate spheroid is irrotational leading to,

$$\zeta \to 0 \quad \text{as } \xi \to \infty. \tag{8}$$

3. The method of solution

Consider the following expansions for ψ and ζ

$$\psi = \sum_{n=1}^{\infty} f_n(\xi) \int_{\gamma}^{1} P_n(\tau)\,\mathrm{d}\tau, \tag{9}$$

$$\zeta = \sum_{n=1}^{\infty} g_n(\xi) P_n^1(\gamma), \tag{10}$$

where $P_n(\gamma)$ and $P_n^1(\gamma)$ are, respectively, the Legendre and first associated Legendre polynomials of order n with argument $\gamma = \cos\eta$. These functions form a complete orthogonal set in the range $\gamma = -1$ to $\gamma = 1$, Alassar and Badr [4] and Dennis and Walker [5].

Substituting from Equations (9) and (10) in Equations (2) and (3) and multiplying by $P_m^1(\gamma)$ and then integrating over γ from -1 to 1, we obtain the following expressions by using the orthogonality properties of the Legendre functions,

$$\begin{aligned}\frac{\mathrm{d}^2 f_n}{\mathrm{d}\xi^2} - \tanh\xi\frac{\mathrm{d}f_n}{\mathrm{d}\xi} - n(n+1)f_n \;=\; & \cosh\xi\, n(n+1)\left[\sinh^2\xi + \frac{2n^2+2n-3}{(2n-1)(2n+3)}\right] g_n \\ & + \cosh\xi \frac{n(n+1)(n+2)(n+3)}{(2n+3)(2n+5)} g_{n+2} \\ & + \cosh\xi \frac{n(n-1)(n-2)(n+1)}{(2n-1)(2n-3)} g_{n-2},\end{aligned} \tag{11}$$

$$\frac{\mathrm{d}^2 g_n}{\mathrm{d}\xi^2} + \tanh\xi\frac{\mathrm{d}g_n}{\mathrm{d}\xi} + \left[\frac{1}{\cosh^2\xi} - n(n+1)\right] g_n = \frac{\mathrm{Re}}{2} S_n, \tag{12}$$

where,

$$S_n = \frac{1}{\cosh\xi}\left[\sum_{i=1}^{\infty}\sum_{j=1}^{\infty} \alpha_{ij}^n f_i \left(\frac{\mathrm{d}g_j}{\mathrm{d}\xi} - \tanh\xi\, g_j\right) + \sum_{i=1}^{\infty}\sum_{j=1}^{\infty} \beta_{ij}^n g_j \frac{\mathrm{d}f_i}{\mathrm{d}\xi}\right], \tag{13}$$

with the understanding that $g_{-1} = g_0 = 0$ and the coefficients appearing in the series in Equation (13) are defined as:

$$\alpha_{ij}^n = -(2n+1)\sqrt{\frac{j(j+1)}{n(n+1)}} \begin{pmatrix} n & i & j \\ -1 & 0 & 1 \end{pmatrix} \begin{pmatrix} n & i & j \\ 0 & 0 & 0 \end{pmatrix}, \tag{14}$$

$$\beta_{ij}^n = (2n+1)\sqrt{\frac{j(j^2-1)(j+2)}{n(n+1)i(i+1)}} \begin{pmatrix} n & i & j \\ -1 & -1 & 2 \end{pmatrix} \begin{pmatrix} n & i & j \\ 0 & 0 & 0 \end{pmatrix}, \tag{15}$$

where $\begin{pmatrix} j_1 & j_2 & j_3 \\ m_1 & m_2 & m_3 \end{pmatrix}$ are the 3-j symbols, which are defined in the Appendix.

The governing equations are now written in the form of a set of ordinary differential equations with the dependent variables being the coefficients (f_n, g_n) of the series. The resulting Equations (11) and (12) represent two sets of ordinary differential equations, with every set containing an infinite number of equations, as compared to the original two partial differential equations. However, we will solve only few of these equations and yet obtain a highly accurate solution. The boundary conditions associated with these equations are

$$f_n(\xi_o) = \frac{\mathrm{d}f_n}{\mathrm{d}\xi}(\xi_o) = 0, \tag{16}$$

$$f_n(\xi) \to \cosh^2\xi\,\delta_{n1}, \qquad \frac{\mathrm{d}f_n(\xi)}{\mathrm{d}\xi} \to \sinh 2\xi\,\delta_{n1}, \quad g_n(\xi) \to 0 \quad \text{as } \xi \to \infty, \tag{17}$$

where δ_{n1} is the Kronecker delta.

4. The numerical algorithm

The solutions of the functions ψ and ζ are obtained by solution of the Equations (11) and (12) for the functions f_n and g_n and then substitution of the results in the series (9) and (10). Equations (11) and (12) are first truncated after $n = N$ for some N which is to be determined experimentally in order to achieve a highly accurate solution. In doing so, the truncation automatically assigns zero values for all the functions with subscripts greater than N. These functions with subscripts greater than N appear on the right hand side of Equation (11) when solving for the f_n functions with subscripts $n = N-1$ and N. As a starting point, all functions are assigned zero values. Equations (11) and (12) are then solved iteratively. The numerical algorithm is as follows

1. Denoting the right-hand side of Equation (11) by $r_n(\xi)$, it can be rewritten as $\mathrm{d}^2 f_n/\mathrm{d}\xi^2 - \tanh\xi(\mathrm{d}f_n/\mathrm{d}\xi) - n(n+1)f_n = r_n(\xi)$. For each mode n, central differences are used to approximate the space derivatives and the resulting tridiagonal system of equations are then solved for the function f_n. All the functions f_n are obtained sequentially from $n = 1$ to N.
2. Similarly, Equations (12) are then solved for the functions g_n sequentially from $n = 1$ to N. It is important to observe that there are no boundary conditions for the functions g_n at the surface of the spheroid. These values which are required to complete the integration of Equations (12) are set to zero for the first iteration and then updated in subsequent iterations as described in the next step.

3. We obtain the boundary values of the functions g_n from Equations (11) by approximating the space derivative $\mathrm{d}^2 f_n/\mathrm{d}\xi^2$ by central differences. The following formula is obtained

$$\cosh\xi_o n(n+1)\left[\sinh^2\xi_o + \frac{2n^2+2n-3}{(2n-1)(2n+3)}\right] g_n(\xi_o)$$
$$+\cosh\xi_o \frac{n(n+1)(n+2)(n+3)}{(2n+3)(2n+5)} g_{n+2}(\xi_o)$$
$$+\cosh\xi_o \frac{n(n-1)(n-2)(n+1)}{(2n-1)(2n-3)} g_{n-2}(\xi_o) = \frac{2f_n(\xi_o+h)}{h^2},$$

   where $h = \Delta\xi$. This approximation was successfully used for the elliptic cylinder case by Patel [6] and for the sphere case by Drummond and Lyman [7]. This formula is solved for the functions g_n on the surface of the spheroid (*i.e.* $g_n(\xi_o)$) sequentially from $n = 1$ to N. It is important to understand that at any given instant we use the most recently available information on the functions g_n and f_n. For example, the values of the functions g_{j+2}(j represents any mode from 1 to N) in the last formula which we need when solving for $g_j(\xi_o)$, are taken from previous iterations, while those for the function g_{j-2} are already updated because they are solved for prior to g_j within the same iteration.
4. It was found that a relaxation factor was necessary to determine the functions g_n^m (m refers to the iteration number) according to

$$g_n^m(\xi) = \kappa g_n^m(\xi) + (1-\kappa) g_n^{m-1}(\xi), \tag{18}$$

   where $g_n^{m-1}(\xi)$ are the solutions obtained from the previous iteration, and $0 < \kappa < 1$.
5. Repeat all steps until convergence is reached. The condition set for convergence is $|g_n^m(\xi) - g_n^{m-1}(\xi)| < 10^{-10}$.

The number of points used in the ξ direction is 201 with a space step of 0·025. This sets the outer boundary at a physical distance that ensures that the conditions at infinity are appropriately incorporated in the numerical solution. We examined the effect of the step size on the flow field near the spheroid by comparing the results when using different values. No significant changes in the values of the drag or the surface vorticity were detected by reducing the step size further than the given value. As there is no intrinsic way to determine it, the total number of terms taken in the series was found by numerical experiments. The total number of terms depends on Reynolds number and ξ_o. For higher Reynolds numbers and lower ξ_o, more terms are needed. One way to check the sufficiency of the number of terms taken in the series is to observe the difference in the values of the drag. Figure 2 shows the surface vorticity for the case Re = 0·1 and $\xi_o = 0{\cdot}25$ at different values of N. In this case, the drag values for the cases $N = 6, 8, 10, 12$, and 16 are respectively, 5·14565, 5·15525, 5·15775, 5·15845, and 5·15875 which differ at the maximum by 0·3%. The parameter κ, which is used in the averaging process of the vorticity calculations, was determined through numerical experiments. The parameter is higher for higher Reynolds numbers and is not sensitive to the parameter ξ_o. The number of iterations required for convergence at a tolerance of 10^{-10} ranges betwee 2,000 and 10,000. The higher number of iterations corresponds to the smaller axis ratio. The CPU times depend on the number of terms taken in the series which, in turn, depends on Reynolds number and the axis ratio. Typically 2 to 5 hours were needed for convergence on a 486-PC with a 100-MHz processor.

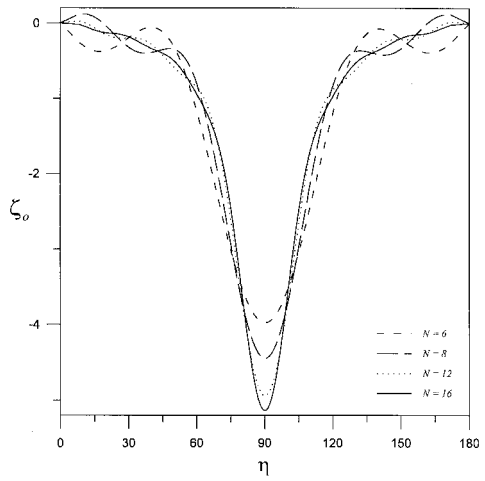

Figure 2. Surface vorticity distribution for the case Re = 0·1, $\xi_o = 0{\cdot}25$ at different N values.

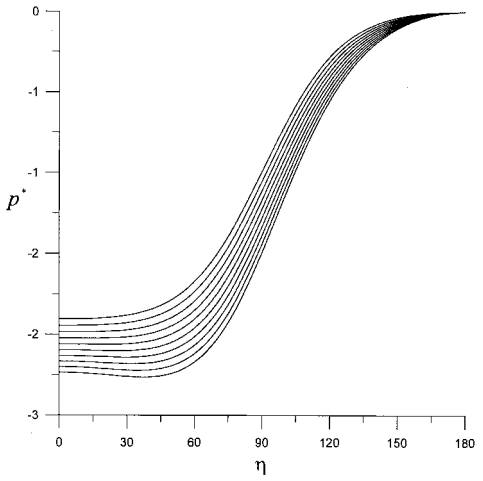

Figure 3. Surface pressure distribution for the case $\xi_o = 1{\cdot}0$, at different Reynolds numbers (Curves from top to bottom are respectively Re = 0·1, 0·2, 0·3, 0·4, 0·5, 0·6, 0·7, 0·8, 0·9, 1·0).

5. Results and discussion

In a typical problem of this nature, the quantities sought are the drag, surface vorticity, surface pressure distribution, and the streamline and vorticity patterns. In what follows, we present these for Reynolds numbers of 0·1, 0·5, and 1·0 at values of ξ_o of 0·25, 0·5, 0·75, 1·0, 1·25, and 1·5.

The drag exerted by the fluid on the spheroid, denoted by D is related to the dimensionless coefficient C_D by,

$$C_D = \frac{Dc'}{A\mu U_o}, \tag{19}$$

where $A(= \pi c'^2 \cosh^2 \xi)$ is the spheroid projected area. The drag coefficient is composed of two parts, one due to friction and the other due to pressure. We may then write,

$$C_D = C_{DF} + C_{DP}. \tag{20}$$

By integrating these forces over the surface of the spheroid, we get

$$C_{DF} = -2 \tanh \xi_o \int_o^\pi \zeta(\xi_o, \eta) \sin^2 \eta \, d\eta, \tag{21}$$

$$C_{DP} = -\frac{c'}{\mu U_o} \int_0^\pi p'(\xi_o, \eta) \sin 2\eta \, d\eta, \tag{22}$$

where p' is the dimensional pressure. By applying Navier-Stokes equations on the surface of the spheroid, one can show that

$$\left(\frac{\partial p}{\partial \eta}\right)_{\xi=\xi_o} = \left[\frac{\partial \zeta}{\partial \xi} + \tanh \xi \zeta\right]_{\xi=\xi_o}, \tag{23}$$

where $p = p'c'/\mu U_o$. Using Equation (23) together with Equation (10), the drag components can be expressed as

$$C_{DF} = \frac{8\tanh\xi_o}{3} g_1(\xi_o, t), \tag{24}$$

$$C_{DP} = -\frac{4}{3}\left[\tanh\xi_o g_1(\xi_o, t) + \frac{\partial g_1}{\partial\xi}(\xi_o, t)\right]. \tag{25}$$

As indicated by Equations (24) and (25), the drag depends on the first mode of the series in Equation (10) which, in turn, depends on the other modes. The drag formula given by Payne and Pell [2] takes the form

$$C_{D1} = \frac{2B}{3\cosh\xi_o}, \tag{26}$$

and that modified by Breach [3] is

$$C_{D2} = \frac{2B}{3\cosh\xi_o}\left[1 + \frac{B\mathrm{Re}}{48} + \frac{B^2\mathrm{Re}^2}{1440}\log(\mathrm{Re}/2) + O(\mathrm{Re}^2)\right], \tag{27}$$

$$\text{where } B = \frac{12}{\cosh\xi_o[\sinh\xi_o + (1-\sinh^2\xi_o)\cot^{-1}(\sinh\xi_o)]}. \tag{28}$$

The dimensionless pressure distribution around the oblate spheroid can be obtained by integrating Equation (23) which results in

$$p^* = p_\eta - p_\pi = \int_\pi^\eta \left(\frac{\partial\zeta}{\partial\xi} + \tanh\xi\,\zeta\right)_{\xi=\xi_o} \mathrm{d}\eta, \tag{29}$$

and by using Equation (10), one can prove that

$$p^*(\eta, t) = \sum_{n=1}^{N}[P_n(\cos\eta) - (-1)^n]\left[\frac{\partial g_n}{\partial\xi}(\xi_o, t) + \tanh\xi_o g_n(\xi_o, t)\right]. \tag{30}$$

Figure 3 shows the surface pressure distributions for the case $\xi_o = 1{\cdot}0$ when Re $=$ 0·1, 0·2, 0·3, 0·4, 0·5, 0·6, 0·7, 0·8, 0·9, and 1·0. As Re increases, the difference in the pressure between the front and the rear stagnation points increases. Figure 4 shows the variation of the corresponding surface vorticity. The drag coefficients for the range of parameters considered in this study along with those from Equations (26) and (27) are listed in Table 1. As Re increases, the computed drag coefficients increase with both C_{D1} and C_{D2} underestimating the drag values. C_{D2} which modifies the Stokes drag presented by C_{D1} is closer to the present numerical solution. It is useful to investigate the quantities $(C_D - C_{D1})/(C_D)^*100$ and $(C_D - C_{D2})/(C_D)^*100$ which measure the relative deviation of the drag formulae given by Payne and Pell [2], and Breach [3] from the present study. At low Re, there is a good agreement between C_{D1}, C_{D2}, and C_D. As Re increases, the values depart from each other with C_{D2} being closer to C_D. If an error of 5% can be accepted, a range of validity for C_{D1}, and C_{D2} can be stated. The formula for C_{D1} is valid for Re $\leqslant 0{\cdot}3$ while that of C_{D2} is valid for higher Reynolds numbers provided that a proper restriction on ξ_o is imposed.

Table 1. Comparison of C_D with Equations (26) and (27).

Re	ξ_o	C_{DF}	C_{DP}	C_D	C_{D1} Equation (26)	C_{D2} Equation (27)	$\frac{C_D-C_{D1}}{C_D}*100$	$\frac{C_D-C_{D2}}{C_D}*100$
0·1	0·25	1·5054	3·6534	5·1588	5·042	5·117	2·26	0·81
0·1	0·50	2·2068	2·6866	4·8934	4·783	4·857	2·26	0·74
0·1	0·75	2·3853	2·0286	4·4139	4·307	4·376	2·42	0·86
0·1	1·00	2·2553	1·5551	3·8104	3·706	3·767	2·74	1·14
0·1	1·25	1·9804	1·2033	3·1837	3·082	3·133	3·19	1·59
0·1	1·50	1·6652	0·9369	2·6021	2·503	2·545	3·81	2·19
0·5	0·25	1·5770	3·8295	5·4065	5·042	5·378	6·74	0·53
0·5	0·50	2·3275	2·8363	5·1638	4·783	5·111	7·37	1·02
0·5	0·75	2·5390	2·1623	4·7013	4·307	4·610	8·39	1·94
0·5	1·00	2·4283	1·6778	4·1061	3·706	3·972	9·74	3·27
0·5	1·25	2·1618	1·3175	3·4793	3·082	3·306	11·42	4·98
0·5	1·50	1·8470	1·0440	2·8910	2·503	2·686	13·42	7·09
1·0	0·25	1·6605	4·0390	5·6995	5·042	5·714	11·54	−0·25
1·0	0·50	2·4625	3·0075	5·4700	4·783	5·439	12·56	0·57
1·0	0·75	2·7045	2·3110	5·0155	4·307	4·913	14·13	2·04
1·0	1·00	2·6125	1·8140	4·4265	3·706	4·238	16·28	4·26
1·0	1·25	2·3530	1·4440	3·7970	3·082	3·530	18·83	7·03
1·0	1·50	2·0385	1·1635	3·2020	2·503	2·869	21·83	10·40

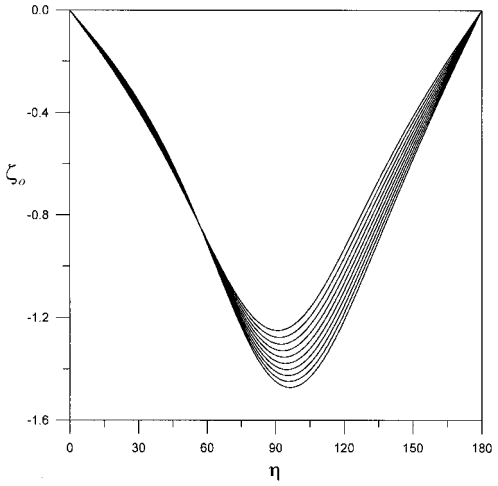

Figure 4. Surface vorticity distribution for the case $\xi_o = 1{\cdot}0$, at different Reynolds numbers (Curves from top to bottom are, respectively, Re = 0·1, 0·2, 0·3, 0·4, 0·5, 0·6, 0·7, 0·8, 0·9, 1·0).

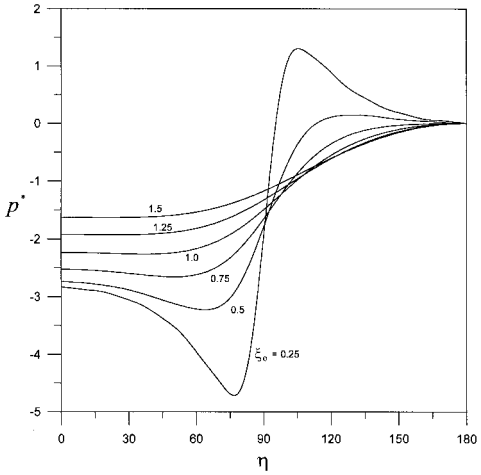

Figure 5. Surface pressure distribution for the case Re = 1·0 at different ξ_o values.

The effect of ξ_o on the pressure distribution and the surface vorticity can be seen in Figures 5 and 6. The Figures which show the results at Re = 1·0 when $\xi_0 = 0{\cdot}25$, 0 ·5, 0·75, 1·0, 1·25,

and 1·5 indicate that when ξ_o decreases, the surface vorticity increases and a positive pressure gradient may be expected. $\xi_o = 0$ corresponds to the circular disk case at which a singular behavior of the pressure gradient is expected. Figure 7 shows the surface pressure distributions for the case of $\xi_o = 0{\cdot}25$. The corresponding analytical surface pressure distribution by Payne and Pell [2] is also plotted on the same figure. An excellent agreement between the present study and that of Payne and Pell can be observed at $\mathrm{Re} = 0{\cdot}1$.

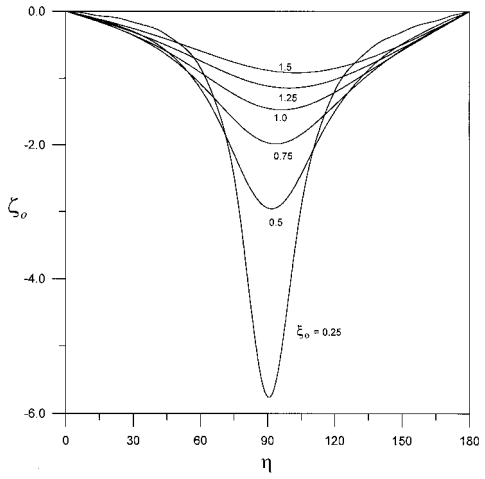

Figure 6. Surface vorticity distribution for the case $\mathrm{Re} = 1{\cdot}0$, at different ξ_o values.

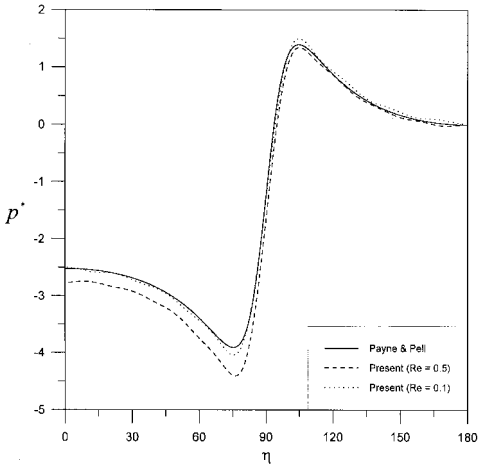

Figure 7. Surface pressure distribution for the case of $\xi_o = 0{\cdot}25$, and comparisons with the analytical solution by Payne and Pell.

Figure 8 shows the streamline and vorticity patterns for the cases $\mathrm{Re} = 0{\cdot}1$ and $1{\cdot}0$ when $\xi_o = 0{\cdot}25$ and $0{\cdot}75$. As expected, no separation occurs at these low Re values. The symmetry of the equi-vorticity lines at $\mathrm{Re} = 1{\cdot}0$ is slightly distorted at $\mathrm{Re} = 1{\cdot}0$.

6. Conclusions

The series-truncation method by which the steam function and vorticity are expanded in terms of Legendre functions has been used to investigate the flow past oblate spheroids at low Reynolds numbers. The governing partial differential equations were transformed into two sets of ordinary differential equations in the radial direction. A second-order accurate finite-difference scheme was then used to solve these equations. The numerically computed drag showed an excellent agreement with the analytical drag formulae given by Payne and Pell [2] and Breach [3] at low Reynolds numbers. As Reynolds number increases, the calculated solution departed from these analytical solutions. An estimate of the range of validity of the analytical solutions has been made.

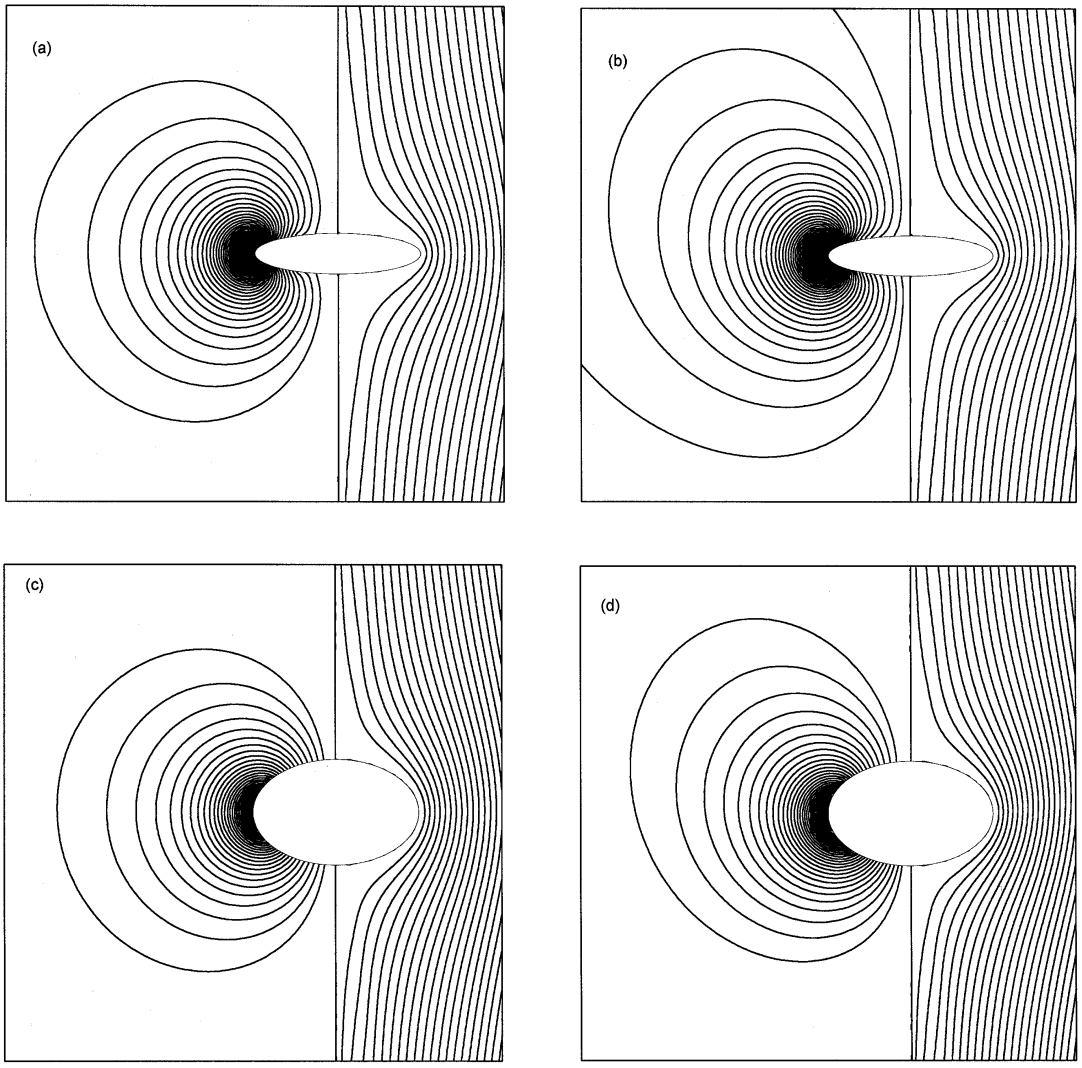

Figure 8. Streamline (right) and vorticity (left) for the cases (a) Re $= 0{\cdot}1$, $\xi_o = 0{\cdot}25$, (b) Re $= 1{\cdot}0$, $\xi_o = 0{\cdot}25$, (c) Re $= 0{\cdot}1$, $\xi_o = 0{\cdot}75$, (d) Re $= 1{\cdot}0$, $\xi_o = 0{\cdot}75$.

7. Appendix

The 3-j symbols $\begin{pmatrix} j_1 & j_2 & j_3 \\ m_1 & m_2 & m_3 \end{pmatrix}$ are transformation coefficients that appear in the problem of adding angular momenta. They represent the probability amplitude that three angular momenta j_1, j_2, and j_3 with projections m_1, m_2, and m_3 are coupled to yield zero angular momentum. They are related to the famous Clebsch-Gordan coefficients (C). These symbols,

however, possess simpler symmetry properties. The relation between 3-j symbols and the Clebsch-Gordan coefficients is given by

$$\begin{pmatrix} j_1 & j_2 & j_3 \\ m_1 & m_2 & m_3 \end{pmatrix} = (-1)^{j_3+m_3+2j_1} \frac{1}{\sqrt{2j_3+1}} C^{j_3 m_3}_{j_1 - m_1 \, j_2 - m_2}.$$

Many representations of the 3-j symbols are available. They may be represented by the square 3×3 array of the Regge R-symbol, by algebraic sums, or in terms of the generalized hypergeometric function of unit argument $({}_3F_2)$. The following formula should give a flavor of the many representations available

$$\begin{aligned} C^{c\gamma}_{a\alpha b\beta} &= \delta_{\gamma,\alpha+\beta} \frac{\Delta(abc)}{(a+b-c)!(-b+c+\alpha)!(-a+c-\beta)!} \\ &\quad \times \left[\frac{(a+\alpha)!(b-\beta)!(c+\gamma)!(c-\gamma)!(2c+1)!}{(a-\alpha)!(b+\beta)!} \right]^{1/2} \\ &\quad \times {}_3F_2 \left[\begin{matrix} -a-b+c, -a+\alpha, -b-\beta \\ -a+c-\beta+1, -b+c+\alpha+1 \end{matrix} \middle| 1 \right] \end{aligned}$$

where

$$\Delta(abc) = \left[\frac{(a+b-c)!(a-b+c)!(-a+b+c)!}{(a+b+c+1)!} \right]^{1/2}$$

For detailed discussion, representations, properties, and tabulated values, the reader is referred to Varshalovich *et al.* [8, pp. 235–411].

Acknowledgement

The authors which to acknowledge the support of King Fahd University of Petroleum and Minerals.

References

1. C. J. Lawrence and S. Weinbaum, The force on an axisymmetric body in linearized, time-dependent motion: a new memory term. *J. Fluid Mech.* 171 (1986) 209–218.
2. L. E. Payne and W. H. Pell, The Stokes flow problem for a class of axially symmetric bodies. *J. Fluid Mech.* 7 (1960) 529–549.
3. D. R. Breach, Slow flow past ellipsoids of revolution. *J. Fluid Mech.* 10 (1961) 306–314.
4. R. S. Alassar and H. M. Badr, Oscillating viscous flow over a sphere. *Comp. Fluids* 26 (1997) 661–682.
5. S. C. R. Dennis and J. D. A Walker, Calculation of the steady flow past a sphere at low and moderate Reynolds numbers. *J. Fluid Mech.* 48 (1971) 771–789.
6. V. C. Patel, Flow around the impulsively started elliptic cylinder at various angles of attack. *Comp. Fluids* 9 (1981) 435–462.
7. C. K. Drummond and F. A. Lyman, Mass transfer from a sphere in an oscillating flow with zero mean velocity. *Comp. Mech.* 6 (1990) 315–326.
8. D. A. Varshalovich, A. N. Moskalev and V. K. Khersonskii, *Quantum Theory of Angular Momentum.* Singapore: World Scientific (1988) 514 pp.